An Energetics Analysis of Forecast Experiments with the NCAR General Circulation Model[1]

WAYMAN E. BAKER[2] AND ERNEST C. KUNG

Department of Atmospheric Science, University of Missouri,[3] Columbia 65201

RICHARD C. J. SOMERVILLE

National Center for Atmospheric Research[4] Boulder, Colo. 80307

(Manuscript received 18 October 1977, in final form 7 December 1977)

ABSTRACT

The energetics in numerical weather forecast experiments with the NCAR general circulation model have been analyzed. The 6-layer, 5-degree, second-generation global model was used to make two 10-day forecasts with the same initial conditions. The two experiments differed primarily in the methods of convective parameterization.

Hemispheric integrals of the model energies and energy transformations are presented in the context of their approach to a quasi-equilibrium climatology. Spectral and spatial analyses of the eddy energies and transformations provide further insight into the model response to the initial conditions. After the initial adjustment, the eddy kinetic energy appears to lag the conversion from eddy available potential energy to eddy kinetic energy by at least 48 h in the long waves (wavenumbers 1–4) and by approximately 24 h in the baroclinic waves (wavenumbers 5–7), whereas little or no time lag is apparent in the short waves (wavenumbers 8–12).

The sensitivity of the forecast energetics to two different convective parameterizations is also examined. There is little appreciable difference between the two experiments in the eddy kinetic energy integrals during the first 36 h of the forecast, but temporal patterns of the eddy transformations are distinctly different after 12 h.

1. Introduction

In a previous paper (Baker *et al.*, 1977; hereafter referred to as BKS) we presented the results of a comprehensive diagnosis of the energetics of the NCAR general circulation model (GCM). The analysis was based on a set of 30-day mean values obtained from January and July simulation experiments with two different convective parameterizations.

In this study, we analyze two 10-day, real-data forecasts with the NCAR GCM. The purpose of this investigation is to examine the relaxation of the NCAR GCM to its quasi-equilibrium climatology in terms of various energies and transformations. The forecasts were begun from analyzed observational data. Adjustment of models to imperfect initialization may take several days (Miyakoda *et al.*, 1969). In the case of the model utilized in this study, a 10-day period appears to be long enough to permit a fairly complete relaxation of the model to its quasi-equilibrium climatology.

Previous studies have compared time-mean forecast results with time-mean observational estimates to assess forecast skill (e.g., Miyakoda *et al.*, 1969, 1972; Druyan *et al.*, 1975). In this study, however, we compare daily forecast energetics with those from an arbitrarily chosen time period from the quasi-equilibrium experiments reported in BKS. As discussed in BKS, the 30-day mean energetics from simulation experiments with two different convective parameterizations are quite distinct. Deficiencies related to inaccurate parameterization of physical processes are known to be important sources of error in present-day numerical weather prediction models (e.g., Miyakoda, 1975; Robert, 1976; Somerville, 1976). At least some of the deficiencies in climate simulation are also attributable to these inadequate parameterizations. Therefore, we also examine the sensitivity of the forecast energetics to differences in convective parameterization. Other investigators who have also used energetics to evaluate

[1] Research supported jointly by the National Center for Atmospheric Research and by the Climate Dynamics Research Section, National Science Foundation.

[2] Currently at NCAR for doctoral research supported by a University Corporation for Atmospheric Research graduate assistantship.

[3] Contribution from the Missouri Agricultural Experiment Station, Journal Series Number 7990.

[4] The National Center for Atmospheric Research is sponsored by the National Science Foundation.

0027-0644/78/0311-0323$06.50

TABLE 1. Symbols and definitions used in this paper.

λ	longitude
ϕ	latitude
p	pressure
t	time
a	radius of the earth
z	height above sea level
$\mathbf{V}$	two-dimensional wind vector
∇	horizontal del operator
u	eastward wind speed $[=a\cos\phi d\lambda/dt]$
v	northward wind speed $[=ad\phi/dt]$
w	vertical wind speed $[=dz/dt]$
ω	vertical p velocity $[=dp/dt]$
ρ	density
α	specific volume $[=1/\rho]$
T	temperature
R	gas constant
c_p	specific heat at constant pressure
g	acceleration of gravity
Φ	geopotential $[=gz]$
n	zonal wavenumber
f	arbitrary function
$\hat{f}$	zonal average of f $[=\frac{1}{2\pi}\int_0^{2\pi} f d\lambda]$
f'	departure from zonal average $[=f-\hat{f}]$
$\{f\}$	meridional average of f between ϕ_1 and ϕ_2 $[=(\sin\phi_2-\sin\phi_1)^{-1}\int_{\phi_1}^{\phi_2} f\cos\phi d\phi]$
f''	departure from meridional average $[=f-\{f\}]$
γ	global mean static stability parameter, where the integration of $\{T\}$ is from pole to pole, i.e., $\phi_1=-\pi/2$, $\phi_2=\pi/2$ $[=(\{T\}-pc_pR^{-1}\partial\{T\}/\partial p)^{-1}]$

parameterizations in forecast sensitivity studies include Miyakoda *et al.* (1969, 1971), Fischer *et al.* (1973), Miyakoda (1975), Somerville *et al.* (1976) and Williamson (1978).

This study primarily presents an intercomparison of four model integrations: two quasi-equilibrium simulations and two real-data forecasts. The simulations also have been compared with real climatological data in BKS, but in the present paper we have not compared the forecasts with the detailed evolution of the real atmosphere, either in terms of energetics or by means of conventional verification techniques. Such a comparison, preferably employing more than the single case which we treat, would be worthwhile but well beyond the scope of the present study. Even the more limited objective of the present study would be better served by the analysis of additional cases, as any single case is bound to be unrepresentative in some respects.

Section 2 describes the initialization procedure, and the energetics analysis scheme is outlined in Section 3. Spectral and spatial characteristics of the energetics from the real-data forecast experiments are presented and compared with those from the quasi-equilibrium simulation experiments in Sections 4 and 5. Table 1 defines the symbols used in this paper and Table 2 defines the energies and transformations.

2. Initialization procedure

The model used in this study is the 6-layer, 5-degree, second-generation, global NCAR GCM discussed by Kasahara and Washington (1971) and Washington and Williamson (1977). Two 10-day forecast experiments were made with the GCM with different convective parameterizations.

In Experiment 1 (referred to as Version A in BKS), a convective adjustment scheme was utilized, while Experiment 2 (referred to as Version B in BKS) employed a more elaborate convective parameterization. With the convective adjustment scheme in Experiment 1, unstable lapse rates are readjusted to either the moist adiabatic lapse rate with upward vertical motion or to the dry adiabatic lapse rate with downward vertical motion (Oliger *et al.*, 1970). Experiment 2 utilized a convective scheme originally developed by Kuo (1965) and modified by Krishnamurti and Moxim (1971). Additional details on the modified Kuo scheme are given by Washington *et al.* (1977). As was stated in BKS, these two model versions also differed in several minor respects other than convective parameterization. However, independent tests (Washington *et al.*, 1977) demonstrate that differences in model energetics are dominated by the differences in convective parameterization. Therefore, we refer to Experiments 1 and 2 in this study simply as experiments with different convective parameterizations. The two convective schemes lead in some instances to markedly different energetics results. However, the convective parameterization in Experiment 2 is sufficiently complicated that additional

TABLE 2. Definitions of energies and energy transformations.

Energies and energy transformations	Definitions
K	kinetic energy
K_M	mean kinetic energy
K_E	eddy kinetic energy
$K(n)$	K_E at wavenumber n
P	available potential energy
P_M	mean available potential energy
P_E	eddy available potential energy
$P(n)$	P_E at wavenumber n
$C(K_E,K_M)$	conversion from K_E to K_M
$M(n)$	conversion of $K(n)$ to K_M
$C(P_M,P_E)$	conversion of P_M to P_E
$R(n)$	conversion of P_M to $P(n)$
$C(P,K)$	conversion of P to K
$C(P_M,K_M)$	conversion of P_M to K_M
$C(P_E,K_E)$, $-\overline{\omega'\alpha'}$	conversion of P_E to K_E (eddy conversion)
$C(n)$	conversion of $P(n)$ to $K(n)$
$L(n)$	rate of transfer of K_E from all other wavenumbers to $K(n)$
$S(n)$	rate of transfer of P_E from all other wavenumbers to $P(n)$
D	dissipation of K
$D(K_M)$	dissipation of K_M
$D(K_E)$	dissipation of K_E
$D(n)$	dissipation of $K(n)$
$G(P_M)$	generation of P_M
$G(P_E)$	generation of P_E
$G(n)$	generation of $P(n)$

sensitivity tests would be needed to clarify the physical reasons for the differences between the two convective schemes. Such tests are beyond the scope of this study.

The initial data used in this study were from 0000 GMT 20 December 1972, as analyzed by the National Meteorological Center (NMC) and archived at NCAR (Jenne, 1975). Other studies of forecast experiments have been made with the same 0000 GMT 20 December 1972 data (e.g., Somerville *et al.*, 1974; Druyan *et al.*, 1975; Baumhefner and Downey, 1976; Somerville *et al.*, 1976). These studies include discussions of the performance of several other models in forecasting from these data.

In compiling the global data set, the then-experimental NMC Hough function analysis (Flattery, 1971) was applied, followed by a straightforward interpolation of the NMC data to the NCAR grid system, without employing any other balancing, filtering or smoothing. Two 10-day, global forecasts were made with these data. Model fields were saved on history tapes written every 12 h from 1200 GMT 20 December 1972 through 0000 GMT 30 December 1972. Forecast energetics calculated from these fields are compared in this study with the energetics from days 73–83 of the simulation experiments reported in BKS. This period was chosen arbitrarily as a representative sample of Versions A and B. The energetics from other time periods in the simulation experiments did not differ significantly from those of days 73–83.

Those quantities computed in this study which depend on ω, specifically $C(P_M,P_E)$, $C(P_E,K_E)$ and $L(n)$, cannot be reliably calculated at day 0, because of the lack of a trustworthy ω field. Initial values for these quantities, therefore, are not plotted.

3. Energetics analysis scheme

The preparation of GCM history tape data for analysis and the energetics analysis scheme are only briefly described below. Additional details on the data analysis may be found in BKS.

To perform the energetics analysis in pressure coordinates, we first interpolated the model fields to constant pressure surfaces. The left-hand side of Fig. 1 illustrates the model fields at the geometric heights used in the interpolation and their approximate location in pressure coordinates. Variables contained in or derivable from history tape data are p and w at the model levels, u, v, T and ρ at the model half-levels, and p_s, w_s, u_s, v_s, T_s and p_s at the s level, which is 10 m above the surface. The variables needed for the energetics analysis and the pressure surfaces analyzed are shown on the right-hand side of Fig. 1. A curve fitting with a spline under tension, developed by Cline (1974), was utilized in performing the vertical interpolation at these analysis levels. A large tension factor was used, such that the interpolation was approximately piecewise linear. After interpolating w to the model half-levels (e.g., 1.5, 4.5, 7.5 km), we obtained ω by using the approximation $\omega \approx -\rho g w$ and we then interpolated ω to the desired pressure surfaces. For our purposes, we set $w_s=0$; consequently, $\omega_s=0$. To facilitate the spectral decomposition of model variables on the pressure surfaces, a spline under tension was again utilized to interpolate for data which were discontinuous because of orography.

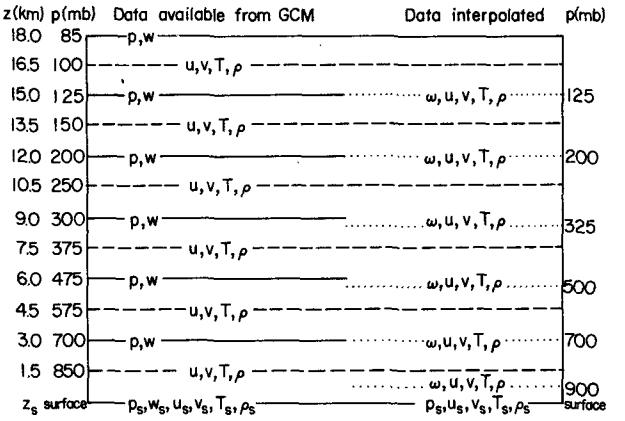

FIG. 1. Vertical distribution of variables in the 6-layer NCAR GCM and the pressure surfaces used for data interpolation.

The Fourier transform pair in this study is identical to that of Saltzman (1970):

$$f(\lambda,\phi,p,t)=\sum_{n=-\infty}^{\infty} F(n,\phi,p,t)e^{in\lambda},$$

$$F(n,\phi,p,t)=\frac{1}{2\pi}\int_0^{2\pi} f(\lambda,\phi,p,t)e^{-in\lambda}d\lambda,$$

where f is an arbitrary function and F its Fourier transform. The actual spectral transformation was by the fast-Fourier transform algorithm of Cooley and Tukey (1965).

The one-dimensional wavenumber formulation of Saltzman (1957, 1970) was utilized in formulating budget equations for kinetic energy and available potential energy. These equations may be written as

$$\frac{\partial K_M}{\partial t}=\sum_{n=1}^{N} M(n)+C(P_M,K_M)-D(K_M), \quad (1)$$

$$\frac{\partial K(n)}{\partial t}=-M(n)+L(n)+C(n)-D(n), \quad (2)$$

$$\frac{\partial P_M}{\partial t}=\sum_{n=1}^{N} R(n)-C(P_M,K_M)+G(P_M), \quad (3)$$

$$\frac{\partial P(n)}{\partial t}=-R(n)+S(n)-C(n)+G(n), \quad (4)$$

where all quantities represent integrals over the entire

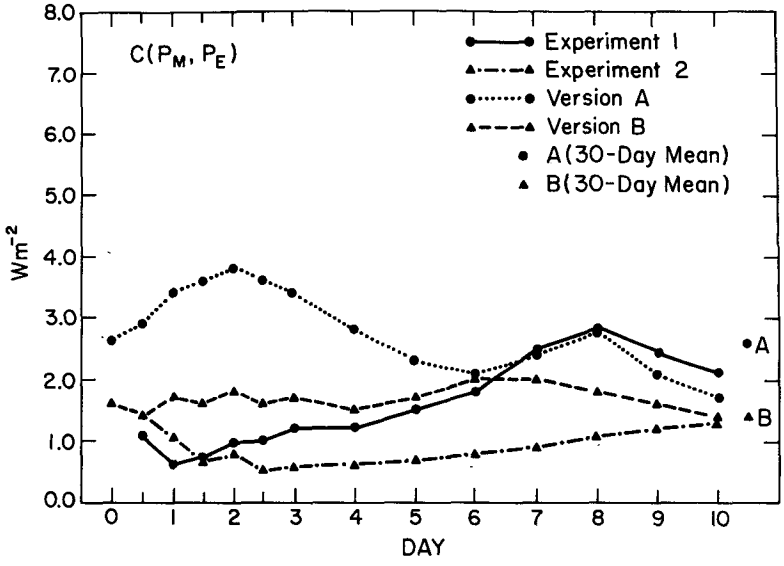

FIG. 2. Time evolution of the conversion of mean to eddy available potential energy, $C(P_M,P_E)$, for two real-data forecasts (Experiments 1 and 2) compared with that for the corresponding simulation experiments (Versions A and B) over the Northern Hemisphere. Single points representing 30-day mean values for Versions A and B are shown at the far right. Fortuitous phase relationships, between the simulation and forecast experiments, in this and following figures, should be disregarded.

mass of the atmosphere. The variables in Eqs. (1)–(4) are as defined by Saltzman (1970) and are listed in Table 2.

The maximum wavenumber computed N is 36 between latitudes 60°S and 60°N, but decreases poleward of 60° because of "grid skipping" (Oliger *et al.*, 1970). The values for eddy quantities are spectral sums over all possible wavenumbers from 1 to 30. Equations for the eddy energies may be obtained by summing (2) and (4) from $n=1$ to N yielding

$$\frac{\partial K_E}{\partial t}=-C(K_E,K_M)+C(P_E,K_E)-D(K_E), \quad (5)$$

$$\frac{\partial P_E}{\partial t}=C(P_M,P_E)-C(P_E,K_E)+G(P_E). \quad (6)$$

In this paper, the results for $L(n)$ from Eq. (2), $C(n)$ from Eqs. (2) and (4), $C(P_E,K_E)$ from Eqs. (5) and (6) and $C(P_M,P_E)$ from Eq. (6) are analyzed. These quantities are readily calculated, generally stable statistically, and yield a fairly reasonable depiction of the model energy budget. In addition, we also present the time evolution of P_E, K_E and K_M. We have not emphasized the results for $C(K_E,K_M)$, a term which is typically small compared to the other conversions in this model, as discussed in BKS.

4. Time evolution of energy variables

Unless otherwise stated, the energetics variables for the NCAR GCM are hemispheric integrals from 0–90°N. The values of these integrals change with time, displaying a characteristic natural variability. However, it is not clear that from a given set of initial conditions the model will inevitably relax to a climatology which is equivalent in all important respects to that of a simulation experiment begun with the model atmosphere initially isothermal and at rest. In the case of Experiment 2, for example, the time integration was extended through day 42. Mean values computed for January 1973 were found to differ from the 30-day mean results, reported in BKS for a perpetual January of Version B, typically by approximately 5–10%. We therefore emphasize the qualitative aspects of the relaxation of Experiments 1 and 2 to the equilibrium climatologies of Versions A and B, respectively. During the first three days of the forecasts, 12 h energetics values help to elucidate the model response to the initial conditions. For the simulation experiments, 12 h values are also plotted for days 73–76 to indicate the 12 h variability after a quasi-equilibrium has been reached. It should be stressed that the particular 11-day period (days 73–83) from the simulation experiments was selected arbitrarily as a representative sample and that no significance should be attached to this choice of days or to fortuitous correspondence between the details of the evolutions of forecasts and simulations.

In Fig. 2, the conversion of mean to eddy available potential energy $C(P_M,P_E)$ is plotted as a function of time for the two forecast experiments and compared with that from the two simulation experiments. The 30-day mean values for the simulation experiments are

TABLE 3. Vertical distribution of global mean temperature (K) through the forecast period. NMC observations for 0000 GMT 20 December 1972 are from the NCAR data library. 30-day mean values are from simulation results (Baker *et al.*, 1977).

		Day											
	0	0.5		1.0		2.0		5.0		10.0		30-day mean	
Pressure level (mb)	NMC observations	Exp 1	Exp 2	Exp 1	Exp 2	Exp 1	Exp 2	Exp 1	Exp 2	Exp 1	Exp 2	Version A	Version B
125	211	212	213	212	214	212	215	212	217	213	222	214	229
200	218	219	220	219	221	219	223	220	226	221	231	221	236
325	236	238	238	237	238	237	239	238	240	239	242	239	247
500	257	257	257	257	256	257	255	256	254	256	254	255	256
700	272	272	272	272	272	272	272	271	270	270	269	269	269
900	283	281	284	282	285	282	285	282	284	282	284	281	283
Surface	285	282	285	284	286	284	286	284	286	284	285	284	285

also shown on the right-hand side of Fig. 2. $C(P_M,P_E)$ decreases sharply in Experiment 1 in the first 24 h of the forecast and then recovers to a maximum at day 8. After day 6, $C(P_M,P_E)$ in Experiment 1 approaches the conversion level of Version A, which has a 30-day mean value (days 73–102) of 2.6 W m^{-2}. In Experiment 2, $C(P_M,P_E)$ decreases through the first 36 h of the forecast, although the rate of decrease in the first 24 h is not as sharp as that in Experiment 1, probably because of the large amounts of latent heat released in the convective parameterization in Experiment 2 (see discussion of Version B in BKS). After 60 h, $C(P_M,P_E)$ slowly increases to a maximum at day 10 in Experiment 2, although the relaxation to a climatological mean appears to be slower in Experiment 2 than in Experiment 1. The 30-day mean results for Version B were obtained from days 61–90 with a value for $C(P_M,P_E)$ of 1.4 W m^{-2}. Different time periods were analyzed in the simulation experiments because of incomplete history tape data. However, in comparing results from other time periods for each case, we found no significant differences from the 30-day mean values reported in this paper.

The time evolution of $C(P_M,P_E)$ is reflected in the approach of the temperature structure of the model atmospheres to the mean climatology in the two experiments. In Table 3, vertical profiles of the global mean temperature in the two experiments are presented and compared with NMC observational data and with 30-day mean values for Versions A and B from BKS. Above 500 mb the global mean temperature in Experiment 1 is already very close to that in Version A at 10 days, while a significant difference still exists at day 10 between Experiment 2 and Version B. This is consistent with the slower rate of approach of $C(P_M,P_E)$ to the climatological mean in Experiment 2.

The time evolution of the eddy available potential energy P_E is shown in Fig. 3. In Experiment 1, P_E decreases through the first six days of the forecast. After day 6, an increase occurs with a maximum at day 8 similar to that noted for $C(P_M,P_E)$. The decline in P_E

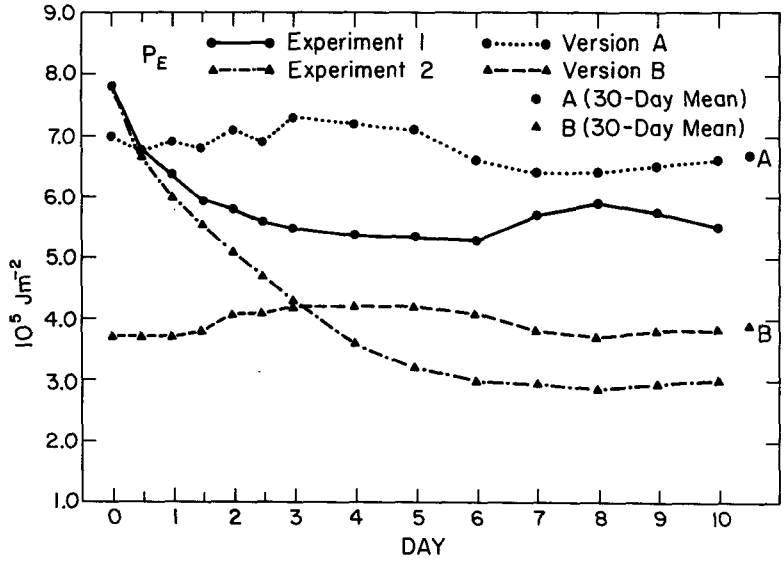

FIG. 3. Time evolution of the eddy available potential energy P_E.

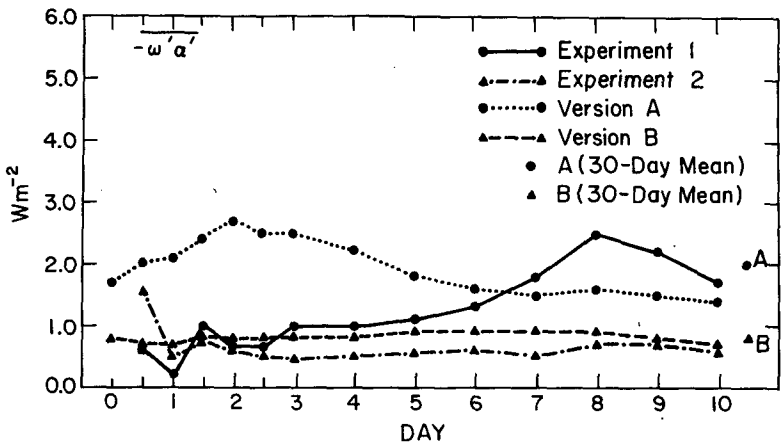

FIG. 4. Time evolution of the eddy conversion $-\overline{\omega'\alpha'}$.

is much sharper in Experiment 2 than in Experiment 1 in the first six days of the forecast, and the decrease continues through day 8. After day 8, P_E slowly increases in a manner similar to that observed for $C(P_M, P_E)$. At day 10, the values of P_E in both experiments are still significantly below the means of 6.7×10^5 and 3.9×10^5 J m^{-2} shown on the right-hand side of Fig. 3 for Versions A and B, respectively.

The eddy conversion $-\overline{\omega'\alpha'}$ is plotted as a function of time in Fig. 4. In Experiment 1, $-\overline{\omega'\alpha'}$ peaks at day 8, in a manner similar to the pattern noted for $C(P_M,P_E)$ and P_E. After day 6, $-\overline{\omega'\alpha'}$ begins to approach the climatological mean for Version A of 2.0 W m^{-2}. The temporal behavior of $-\overline{\omega'\alpha'}$ in Experiment 2 is distinctly different from that in Experiment 1. The fluctuation in $-\overline{\omega'\alpha'}$ in both experiments during the first 48 h of the forecast is, at least in part, a response to imperfect initial conditions. $-\overline{\omega'\alpha'}$ is stronger in Experiment 2 than in Experiment 1 during the first 24 h, particularly at day 0.5, probably because of the release of latent heat mentioned previously. For the duration of the forecast, there is little appreciable increase in $-\overline{\omega'\alpha'}$ in Experiment 2 with $-\overline{\omega'\alpha'}$ remaining slightly below the climatological mean of 0.8 W m^{-2} in Version B.

Contributions from various ranges of wavenumber to the eddy conversion are illustrated in Figs. 5–7. For convenience, we refer to the range $n=1-4$ as long waves, to $n=5-7$ as baroclinic waves and to $n=8$–12 as short waves. It should be noted that $-\overline{\omega'\alpha'}$ is stronger in Experiment 2 than in Experiment 1 at day 0.5 in all wavenumber groups. During the first 48 h of the forecast, a more pronounced fluctuation in $-\overline{\omega'\alpha'}$ is observed in the long waves than in the baroclinic and

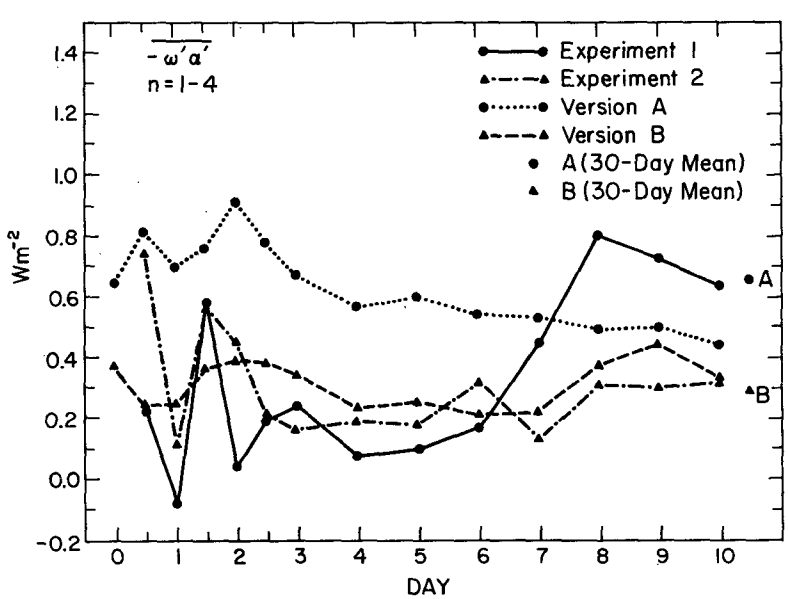

FIG. 5. Time evolution of the long wave (n = 1–4) contribution to $-\overline{\omega'\alpha'}$.

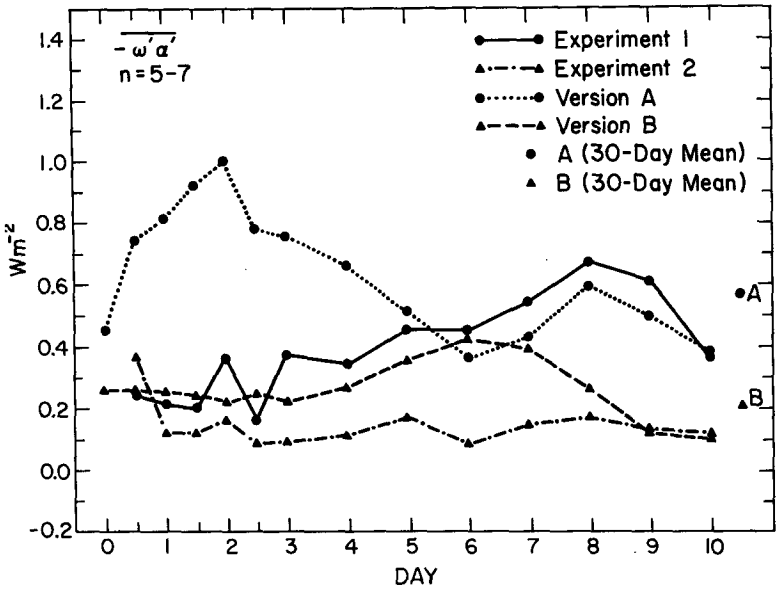

FIG. 6. Time evolution of the baroclinic wave (n=5–7) contribution to $-\overline{\omega'\alpha'}$.

short waves as seen in Figs. 5–7, respectively. In all wavenumber groups, $-\overline{\omega'\alpha'}$ apparently tends to relax to its equilibrium climatology faster in Experiment 2 than in Experiment 1.

The time evolution of the hemispheric eddy and mean kinetic energy are plotted in Fig. 8 and compared with global mean values by Somerville *et al.* (1976) from the Goddard Institute for Space Studies (GISS) model begun with the same initial conditions. As can be seen in the upper part of Fig. 8, the difference between K_E in the two experiments with the NCAR GCM is negligible through the first 36 h of the forecast. In Experiment 1, K_E decreases through the first six days of the forecast, and then increases approaching the 30-day mean for Version A of 4.1×10^5 J m^{-2}. K_E reaches a maximum at day 9, which lags the peak in $-\overline{\omega'\alpha'}$ (Fig. 4) by 24 h. K_E decreases through the first seven days in Experiment 2 with negligible increase thereafter, unlike Experiment 1. After day 5, K_E in Experiment 2 approaches the 30-day mean value for Version B of 1.3×10^5 J m^{-2}. The negligible increase in K_E during the last few days of the forecast in Experiment 2 is probably due to the small increase in $-\overline{\omega'\alpha'}$ (see Fig. 4). In the GISS model, K_E exhibits a temporal pattern

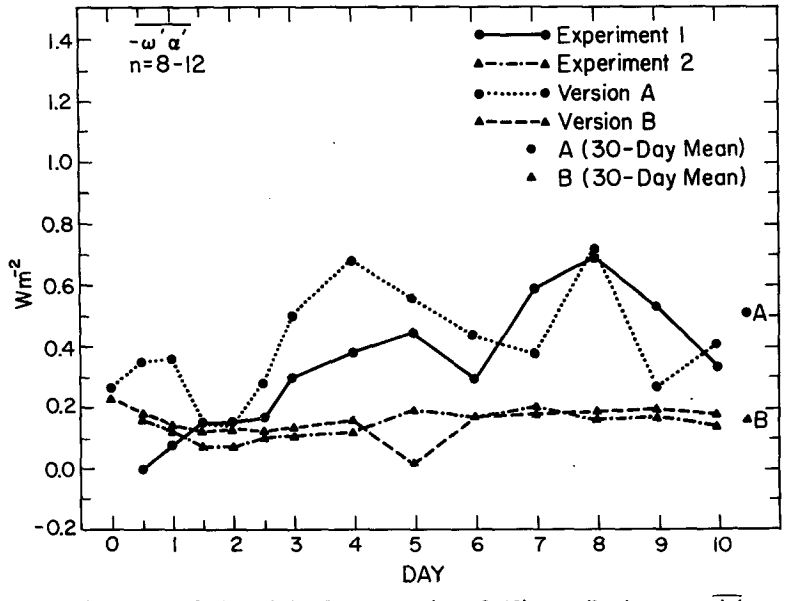

FIG. 7. Time evolution of the short wave (n = 8–12) contribution to $-\overline{\omega'\alpha'}$.

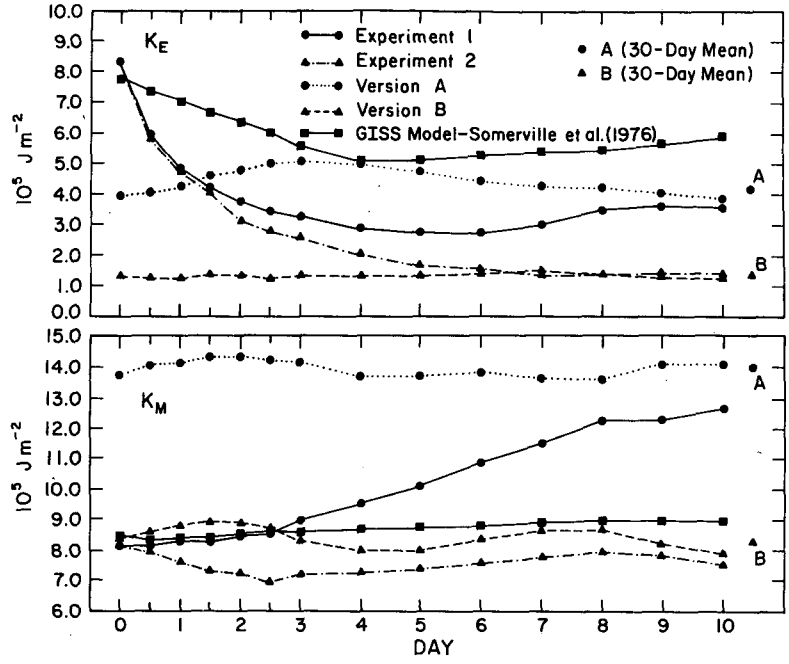

FIG. 8. Time evolution of the eddy and mean kinetic energy compared with global mean values by Somerville *et al.* (1976) from the GISS model begun with the same initial conditions.

similar to that noted for Experiment 1. The rate of initial decrease in the GISS model is much less, however, but a moderate increase in eddy kinetic energy occurs after day 4 for the duration of the forecast, similar to the pattern observed in Experiment 1.

Temporal patterns of K_M are illustrated in the lower part of Fig. 8. In Experiment 2, the mean kinetic energy decreases in the first 60 h of the forecast, whereas K_M in Experiment 1 increases slightly following a pattern similar to that in the first 60 h in the GISS model. After day 2.5, however, the behavior of K_M in Experiment 1 is quite different from that in the GISS model, increasing sharply to approach the 30-day mean value of 14.0×10^5 J m^{-2} in Version A. The significant increase in K_M after day 2.5 in Experiment 1 is probably due to a strengthening of the meridional temperature gradient (see Fig. 4.6 of GCM Steering Committee, 1975). In Experiment 2, K_M increases slowly after day 2.5 approaching after day 5 the climatological mean for Version B of 8.3×10^5 J m^{-2}.

To elucidate further the time variation of K_E in the two experiments, the loss of eddy kinetic energy expressed as a percentage of the initial amount in various ranges of wavenumber is summarized in Table 4. During the first two days of the forecast, both experiments are within 4% of one another in all wavenumber

TABLE 4. Loss of eddy kinetic energy through the forecast period expressed as a percentage of the initial amount in various wavenumber ranges.

	Day													
Wavenumber range	0.5		1.0		1.5		2.0		2.5		3.0		4.0	
	Exp 1	Exp 2	Exp 1	Exp 2	Exp 1	Exp 2	Exp 1	Exp 2	Exp 1	Exp 2	Exp 1	Exp 2	Exp 1	Exp 2
$n=1$–4	20	21	33	37	41	45	48	52	52	58	57	64	64	73
$n=5$–7	43	44	60	61	67	69	71	75	72	80	73	85	77	90
$n=8$–12	51	47	67	63	75	71	75	75	70	77	63	75	51	77

	Day											
Wavenumber range	5.0		6.0		7.0		8.0		9.0		10.0	
	Exp 1	Exp 2	Exp 1	Exp 2	Exp 1	Exp 2	Exp 1	Exp 2	Exp 1	Exp 2	Exp 1	Exp 2
$n=1$–4	68	78	69	81	68	84	64	85	61	85	60	85
$n=5$–7	77	90	73	90	66	90	61	89	55	89	61	89
$n=8$–12	49	77	46	73	37	75	16	76	26	75	42	76

groups. In the first 36 h of the forecast, K_E is slightly stronger in Experiment 1 than in Experiment 2 in the long and baroclinic waves, whereas the opposite is true in the short waves. In Experiment 1, K_E begins to increase after day 2 in the short waves, after day 5 in the baroclinic waves and after day 6 in the long waves. In the temporal behavior of the eddy kinetic energy and eddy conversion, we noted that K_E lagged $-\overline{\omega'\alpha'}$ in Experiment 1 by 24 h with maxima at nine and eight days, respectively. Comparing Table 4 with Figs. 5–7, a time lag of at least 48 h is apparent in the long waves in Experiment 1, while an approximate 24 h time lag appears in the baroclinic waves with $-\overline{\omega'\alpha'}$ reaching a maximum at day 8 and K_E a maximum at day 9. Little or no time lag is apparent in the short waves. The results for the conversion from eddy to mean kinetic energy $C(K_E,K_M)$ (not plotted) also indicate a time lag of approximately 24 h behind $-\overline{\omega'\alpha'}$ in Experiment 1 with $C(K_E,K_M)$ peaking at day 9.

In Fig. 9, the time evolution of the nonlinear interactions for the eddy kinetic energy $L(n)$ is illustrated for Experiment 1 and compared with those for Version A and also with Saltzman's (1970) observational estimates of average winter conditions. Wavenumbers 1, 3, 5 and 7 are analyzed as they have been estimated in the real atmosphere (Saltzman, 1970) to represent two energy sources ($n=5,7$) and two energy sinks ($n=1,3$). Here a particular wavenumber is an energy source if it supplies kinetic energy to other wavenumbers, and an energy sink if it extracts kinetic energy from other wavenumbers. Wavenumber 1 gains energy at the expense of higher wavenumbers throughout the forecast with $L(1)$ generally decreasing beyond day 0.5 and approaching the 30-day mean value of 0.08 W m^{-2} for Version A. Wavenumbers 3, 5 and 7 fluctuate through the forecast as sources and sinks of energy with respect to other wavenumbers, in a manner similar to the behavior of Version A.

As was noted in BKS, the 30-day mean values in Version A for the four wavenumbers that are illustrated are in agreement with Saltzman's estimates at least with respect to the direction of the energy flow. It is apparent, however, with the possible exception of wavenumber 1, that the 30-day mean results in Version A represent residual values of daily negative or positive energy transfers. If the same behavior holds for the real atmosphere as well, whether or not a particular wavenumber is an energy source or sink at a given time would be determined by the ensemble effect of all disturbances at that wavenumber. A particular disturbance would be an energy source or sink, depending on the type of disturbance and stage of development, as indicated by the observational studies of Kung and Baker (1975) and Kung (1977).

5. Latitudinal distribution of eddy kinetic energy and eddy conversion

Latitude-height distributions of the eddy kinetic energy for days 0.5, 2 and 10 of the forecast experiments are illustrated in Fig. 10 and are compared with 30-day mean values from the simulation experiments discussed in BKS. As can be seen in Figs. 10a and 10b, there is

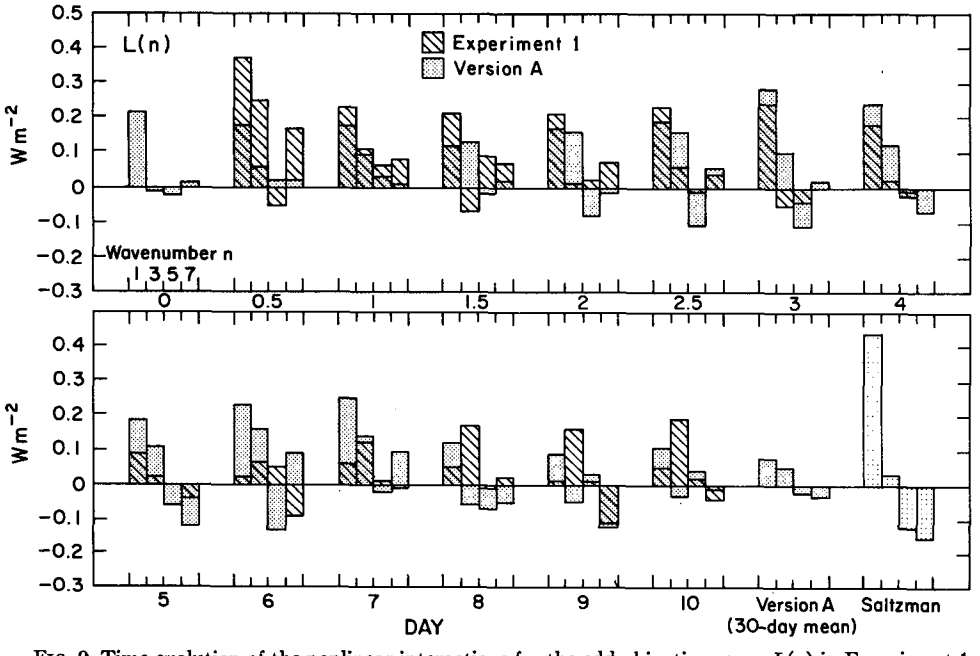

FIG. 9. Time evolution of the nonlinear interactions for the eddy kinetic energy $L(n)$ in Experiment 1 and Version A compared with 30-day mean values for Version A by Baker *et al.* (1977) and with observational estimates by Saltzman (1970) of average Northern Hemisphere winter conditions.

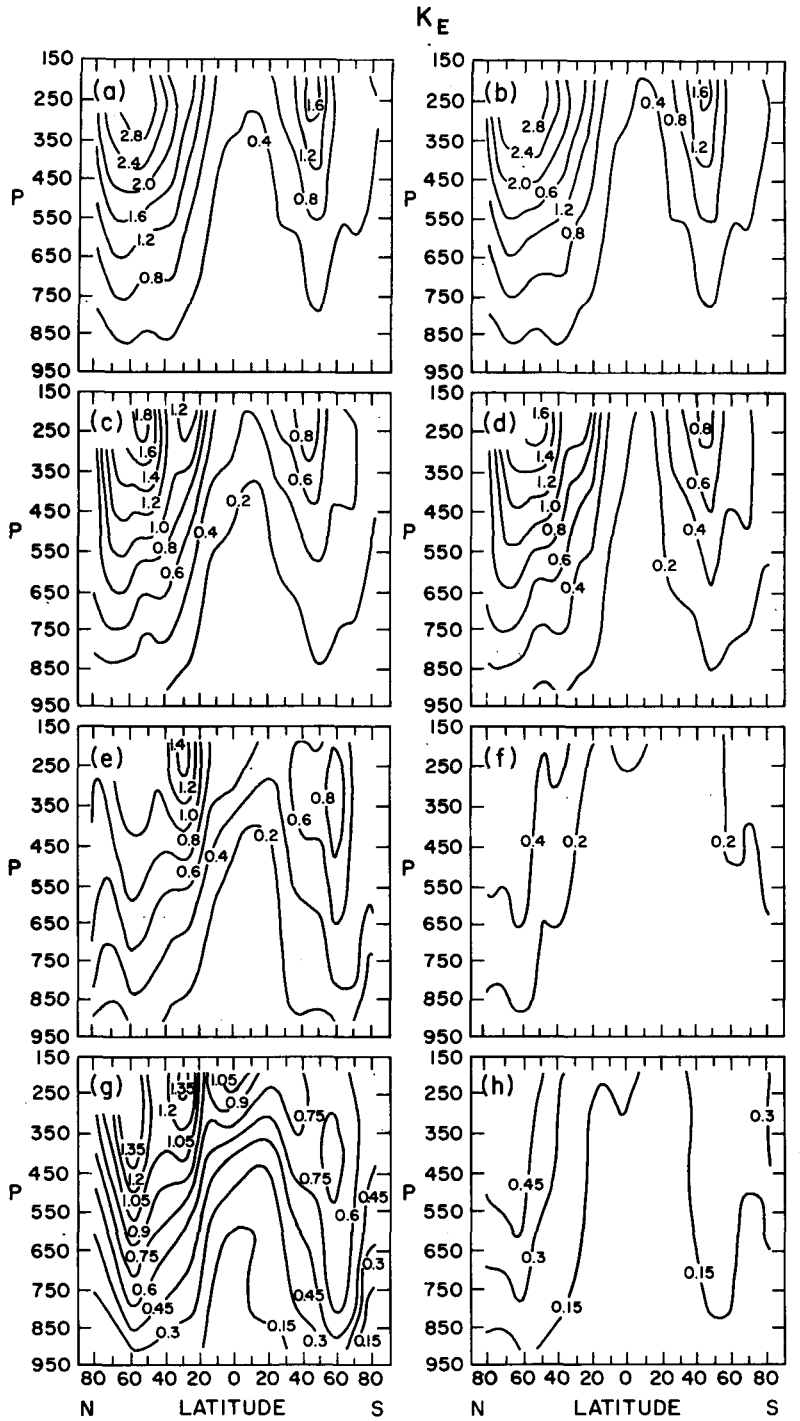

FIG. 10. Latitude-height distribution of the eddy kinetic energy K_E in units of 10^5 J m^{-2} (150 mb)$^{-1}$: (a) Experiment 1, day 0.5; (b) Experiment 2, day 0.5; (c) Experiment 1, day 2; (d) Experiment 2, day 2; (e) Experiment 1, day 10; (f) Experiment 2, day 10; (g) Version A, 30-day mean; (h) Version B, 30-day mean.

little difference in K_E between the two forecast experiments at day 0.5, as was the case for the Northern Hemisphere integrals in Fig. 8. At day 2, on the other hand, Experiment 1 differs noticeably from Experiment 2 (Figs. 10c and 10d). For example, K_E in Experiment 2 is weaker than that in Experiment 1 above 350 mb. The spatial distributions of the eddy kinetic energy for day 10, as illustrated in Figs. 10e and 10f, show a marked difference between Experiments 1 and 2, with K_E substantially stronger in Experiment 1 than in Experiment

2 at all latitudes. Experiment 2 (Fig. 10f) closely resembles the 30-day mean results for Version B in Fig. 10h. As in the January simulation results, K_E in Experiment 2 has a maximum at approximately 70–80°N, which is substantially north of that estimated by Peixóto and Oort (1974) for the real atmosphere

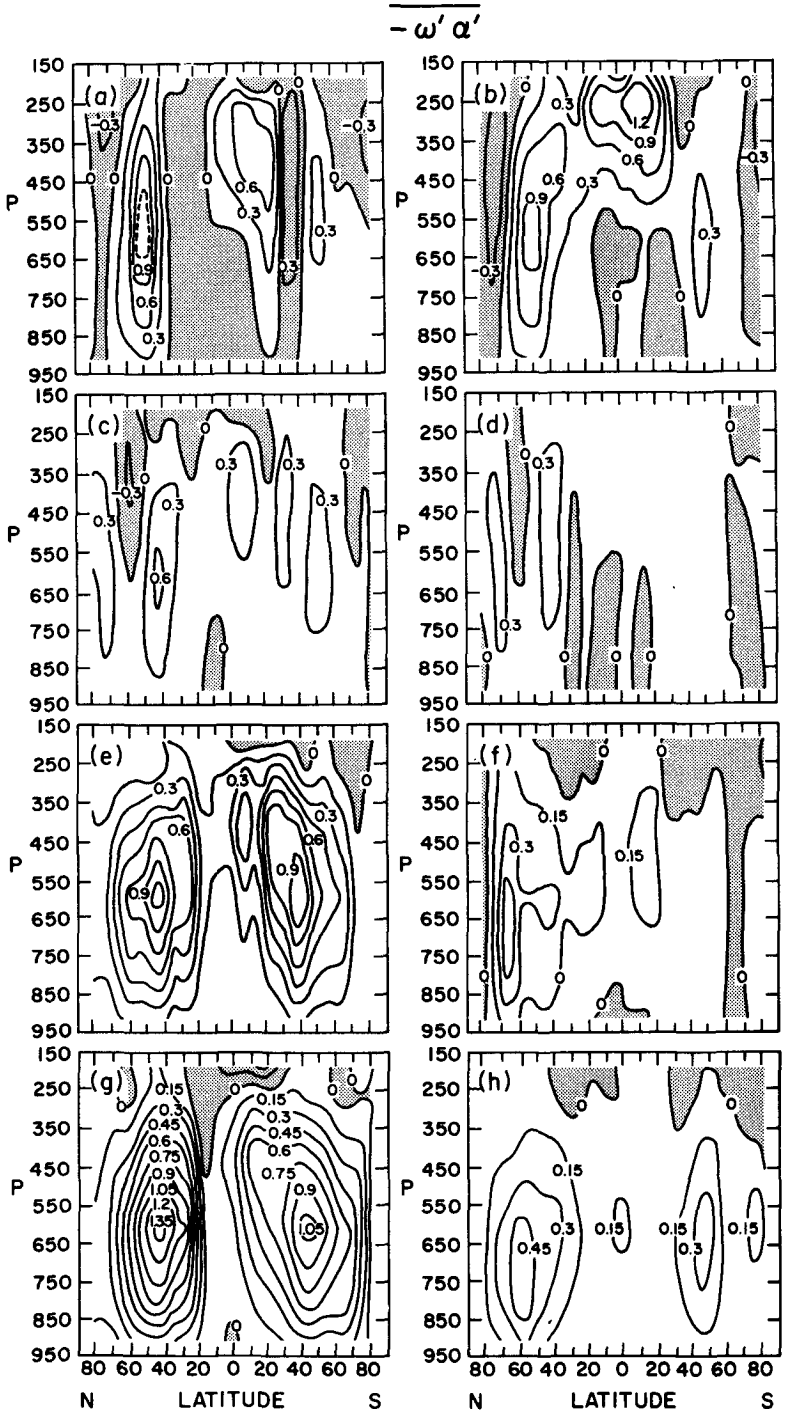

FIG. 11. Latitude-height distribution of the eddy conversion $-\overline{\omega'\alpha'}$ in units of W m^{-2} (150 mb)$^{-1}$: (a) Experiment 1, day 0.5; (b) Experiment 2, day 0.5; (c) Experiment 1, day 2; (d) Experiment 2, day 2; (e) Experiment 1, day 10; (f) Experiment 2, day 10; (g) Version A, 30-day mean; (h) Version B, 30-day mean. Shading indicates negative values.

(Fig. 8c in BKS). In Experiment 1 (Fig. 10e), K_E has a maximum at approximately 25–30°N similar to that in Version A shown in Fig. 10g. Another maximum at approximately 55–60°N in Version A is not as prominent in Experiment 1, however.

Latitudinal distribution diagrams of the eddy conversion are shown in Fig. 11 for the same forecast times as in Fig. 10. At day 0.5, significant differences exist in $-\overline{\omega'\alpha'}$ between the two experiments. There is an intense region of positive conversion in Experiment 2 (Fig. 11b) centered at 250 mb extending approximately from 20°S to 20°N. In Experiment 1 (Fig. 11a), on the other hand, $-\overline{\omega'\alpha'}$ is much weaker in the same region with an area of significantly negative conversion above approximately 200 mb from 5–25°S. The region of strong positive conversion in Experiment 2 at day 0.5 corresponds to a larger Northern Hemisphere value in Experiment 2 than in Experiment 1 as noted in Fig. 4. $-\overline{\omega'\alpha'}$ has a maximum in the upper troposphere in the tropics early in the forecast probably due to the large amounts of latent heat released in the convective parameterization (see discussion of Version B in BKS). At that time the model atmosphere has not yet become stable enough (see Table 3) to suppress vigorous vertical mixing. Experiment 1 (Fig. 11a) has three areas of positive conversion at day 0.5. One is located at approximately 45–55°N centered at 550–600 mb; a similar area may be seen in Experiment 2 (Fig. 11b) although somewhat weaker. A second region of positive conversion in Experiment 1 is located at approximately 10–25°S centered at 400 mb. Both experiments have similar regions of positive $-\overline{\omega'\alpha'}$ at approximately 45–55°S centered at 600 mb, whereas an area of negative conversion at approximately 30–40°S at 350 mb in Experiment 1 is not apparent in Experiment 2.

The intense region of positive $-\overline{\omega'\alpha'}$ noted at day 0.5 in Experiment 2 (from 20°S to 20°N centered at 250 mb) has weakened considerably by day 2 (Fig. 11d), due to the increasingly stable upper troposphere (Table 3). The area of positive conversion in Experiment 1, which was located at day 0.5 at approximately 45–55°N and centered at 550–650 mb, is weaker at day 2 (Fig. 11c), and is located at 40–45°N and centered at 600–650 mb. Similarly, the region of positive $-\overline{\omega'\alpha'}$ which was located at approximately 10–25°S and centered at 400 mb at day 0.5 is now weaker at day 2 and situated at 0–15°S.

The spatial distributions of $-\overline{\omega'\alpha'}$ at day 10, as illustrated in Figs. 11e and 11f, show that Experiments 1 and 2 are distinctly different but resemble the 30-day mean patterns shown for Versions A and B, respectively, in Figs. 11g and 11h. Although $-\overline{\omega'\alpha'}$ is somewhat weaker in Experiment 1 (Fig. 11e) than in Version A (Fig. 11g), there is a maximum at 40–45°N in Experiment 1 as there is in Version A. The eddy conversion in Experiment 2 (Fig. 11f) is very weak with a maximum at 60–70°N, similar to that found in Version B (Fig. 11h).

6. Summary and conclusions

The NCAR GCM has been used to make two 10-day forecasts begun with the same initial conditions, the two experiments differing primarily in the methods of convective parameterization. Energetics of the forecast experiments were examined to investigate the model approach to a quasi-equilibrium climatology.

In general, the experiment which utilizes the modified Kuo convective scheme (Experiment 2) relaxes toward an equilibrium climatology faster than does the experiment which utilizes the convective adjustment scheme (Experiment 1). Specifically, the eddy conversion and eddy and mean kinetic energy in Experiment 2 approach the climatological mean of Version B faster than the approach of those quantities in Experiment 1 to the climatological mean of Version A. However, the eddy available potential energy in both experiments remains significantly below the 30-day mean values of Versions A and B. On the other hand, the conversion from mean to eddy available potential energy in Experiment 1 appears to relax to a climatological mean more quickly than in Experiment 2. This phenomenon is consistent with the fact that, after 10 days, the temperature structure in Experiment 1 is closer to that in Version A than the temperature structure in Experiment 2 is to that in Version B.

The nonlinear interactions for the eddy kinetic energy indicate that wavenumbers 3, 5 and 7 fluctuate through the forecast in Experiment 1 as sources and sinks of energy with respect to other wavenumbers, in a manner similar to that observed in Version A. After the initial adjustment, K_E appears to lag $-\overline{\omega'\alpha'}$ in Experiment 1 by at least 48 h in the long waves and by approximately 24 h in the baroclinic waves, but little or no time lag is detected in the short waves. These results, while plausible, are, of course, based on only one case.

The effects of the different convective parameterizations on the eddy conversion are pronounced. In particular, at day 0.5 an intense region of positive $-\overline{\omega'\alpha'}$ can be seen in Experiment 2 in the upper troposphere from 20°S to 20°N. This is consistent with the temporal pattern of the hemispheric integral and is probably due to the release of latent heat.

Our results demonstrate that the quasi-equilibrium characteristics of the two model climatologies are strongly reflected in the energetics of the real-data forecasts. As noted by GCM Steering Committee (1975), characteristics of the model climatological biases occur sufficiently rapidly to affect forecast skill after a few days. Also, it is clear that spatial and spectral analyses of model energetics are very useful diagnostic tools for understanding model behavior in both types of model applications: climate simulation and short- to medium-range numerical weather prediction. The strong

dependence on convective parameterization shown in this sensitivity study suggests that it would be worthwhile to extend this research to more than a single forecast case and to carry out detailed comparisons between the energetics of model forecasts and those of the corresponding real atmospheric evolutions.

Acknowledgments. The helpful comments and suggestions of Dr. A. Kasahara throughout the course of this study are gratefully acknowledged. Professor B. Saltzman kindly offered assistance on his original formulation of the energetics in the wavenumber domain. We thank Mr. G. Walters for preparing the initial data from the original NMC data set, and Mrs. G. Williamson for supervising the running of the model. Ms. L. Thiel provided assistance with the original NMC data set. We also appreciate the helpful comments of Mr. D. Baumhefner, Mr. T. Bettge, Mr. H. Burgdorf, Mr. T. Mayer, Dr. T. Schlatter, Professor P. Smith, and Dr. W. Washington. We are grateful to Mrs. A. Modahl for preparing the manuscript and to the NCAR graphics department for drafting the figures.

REFERENCES

Baker, W. E., E. C. Kung and R. C. J. Somerville, 1977: Energetics diagnosis of the NCAR general circulation model. *Mon. Wea. Rev.*, **105**, 1384–1401.

Baumhefner, D. P., and P. H. Downey, 1976: Forecast intercomparisons between large-scale numerical weather prediction models. *Ann. Meteor.* (NF), **11**, 205–208.

Cline, A. K., 1974: Scalar- and planar-valued curve fitting using splines under tension. *Commun. Assoc. Comput. Mach.*, **17**, 218–223.

Cooley, J. W., and J. W. Tukey, 1965: An algorithm for the machine calculation of complex Fourier series. *Math. Comput.*, **19**, 297–301.

Druyan, L. M., R. C. J. Somerville and W. J. Quirk, 1975: Extended range forecasts with the GISS model of the global atmosphere. *Mon. Wea. Rev.*, **103**, 779–795.

Fischer, G., E. Heise and V. Renner, 1973: The effect of surface friction on the development of cyclone-waves in a numerical model. *Beitr. Phys. Atmos.*, **46**, 157–181.

Flattery, T. W., 1971: Spectral models for global analysis and forecasting. Air Weather Service Tech. Rep. 242, 42–54.

GCM Steering Committee, 1975: Development and use of the NCAR GCM, A Report of the GCM Steering Committee. NCAR/TN-101+STR, 177 pp.

Jenne, R. L., 1975: Data sets for meteorological research. NCAR Tech. Note IA-111, 169 pp.

Kasahara, A., and W. M. Washington, 1971: General circulation experiments with a six-layer NCAR model, including orography, cloudiness and surface temperature calculations. *J. Atmos. Sci.*, **28**, 657–701.

Krishnamurti, T. N., and W. J. Moxim, 1971: On parameterization of convective and nonconvective latent heat release. *J. Appl. Meteor.*, **10**, 3–13.

Kung, E. C., 1977: Energy sources in middle-latitude synoptic disturbances. *J. Atmos. Sci.*, **34**, 1352–1365.

——, and W. E. Baker, 1975: Energy transformations in middle-latitude disturbances. *Quart. J. Roy. Meteor. Soc.*, **101**, 793–815.

Kuo, H. L., 1965: On formation and intensification of tropical cyclones through latent heat release by cumulus convection. *J. Atmos. Sci.*, **22**, 40–63.

Miyakoda, K., 1975: Weather forecasts and the effect of the subgrid scale processes. *Seminars on Scientific Foundation of Medium Range Weather Forecasts*, European Centre for Medium Range Weather Forecasts, Reading, England, 380–593.

——, G. D. Hembree, R. F. Strickler and I. Shulman, 1972: Cumulative results of extended forecast experiments, I. Model performance for winter cases. *Mon. Wea. Rev.*, **100**, 836–855.

——, J. Smagorinsky, R. F. Strickler and G. D. Hembree, 1969: Experimental extended predictions with a nine-level hemispheric model. *Mon. Wea. Rev.*, **97**, 1–76.

——, R. F. Strickler, C. J. Nappo, P. L. Baker and G. D. Hembree, 1971: The effect of horizontal grid resolution in an atmospheric circulation model. *J. Atmos. Sci.*, **28**, 481–489.

Oliger, J. E., R. E. Wellck, A. Kasahara and W. M. Washington, 1970: Description of the NCAR Global Circulation Model. NCAR Tech. Note TN-56, 94 pp.

Peixóto, J. P., and A. H. Oort, 1974: The annual distribution of atmospheric energy on a planetary scale. *J. Geophys. Res.*, **79**, 2149–2159.

Robert, A., 1976: Sensitivity experiments for the development of NWP models. *Proc. Eleventh Stanstead Seminar*, Publ. Meteor. No. 114, McGill University, 68–81.

Saltzman, B., 1957: Equations governing the energetics of the larger scales of atmospheric turbulence in the domain of wavenumber. *J. Meteor.*, **14**, 513–523.

——, 1970: Large-scale atmospheric energetics in the wavenumber domain. *Rev. Geophys. Space Phys.*, **8**, 289–302.

Somerville, R. C. J., 1976: Sensitivity of large-scale numerical weather forecasts to deficiencies in models. *Ann. Meteor.* (NF), **11**, 266–268.

——, W. J. Quirk, J. E. Hansen, A. A. Lacis and P. H. Stone, 1976: A search for short-term meteorological effects of solar variability in an atmospheric circulation model. *J. Geophys. Res.*, **81**, 1572–1576.

——, P. H. Stone, M. Halem, J. E. Hansen, J. S. Hogan, L. M. Druyan, G. Russell, A. A. Lacis, W. J. Quirk and J. Tenenbaum, 1974: The GISS model of the global atmosphere. *J. Atmos. Sci.*, **31**, 84–117.

Washington, W. M., B. Otto-Bliesner, and G. Williamson, 1977: January and July simulation experiments with the 2.5° latitude-longitude version of the NCAR general circulation model. NCAR Tech. Note TN-123+STR, 100 pp.

——, and D. L. Williamson, 1977: A description of the NCAR global circulation models. *Methods in Computational Physics*, Vol. 17, J. Chang, Ed., Academic Press, 111–172.

Williamson, D. L., 1978: The relative importance of resolution, accuracy, and diffusion in short-range forecasts with the NCAR global circulation model. *Mon. Wea. Rev.*, **106**, 69–88.